Effects of initial soil moisture content on soil water and nitrogen transport under muddy water film hole infiltration

Lihua Liu[1,2], Liangjun Fei[1,2*], Lin Chen[1,2], Kun Hao[1,2], Quanju Zhang[1,2]

(1. *State Key Laboratory of Eco-hydraulics in Northwest Arid Region, Xi'an University of Technology, Xi'an 710048, China*;
2. *Institute of Water Resources and Hydro-electric Engineering, Xi'an University of Technology, Xi'an 710048, China*)

Abstract: Film hole irrigation has been widely adopted as an effective water-saving irrigation technology in the arid and semiarid areas of China.   To investigate the effects of initial soil moisture content (θ_0) on soil water and nitrogen transport characteristics under muddy water film hole infiltration, the laboratory experiments were conducted with muddy water film hole infiltration, using five initial soil moisture content treatments.   The models for describing the relationships between the cumulative infiltration ($I(t)$) and infiltration duration (t); the relationship among the horizontal and vertical migration distances of the wetting front (F_x, F_z), θ_0 and t, were established.   The results showed that the initial soil moisture content had a significant effect on $I(t)$, F_x, F_z and moisture content distribution in the wetted body.   The change of $I(t)$ over t conformed to Kostiakov model.   With the increase of θ_0, the infiltration coefficient (K) gradually decreased. NO_3^--N was mainly distributed in the range of the wetting radius of 15 cm, while NH_4^+-N was mainly distributed in the range of the wetting radius of 8 cm.   This study can provide a theoretical basis and technical support for film hole irrigation.
Keywords: film hole irrigation, muddy water, initial soil moisture content, water and nitrogen transport, water redistribution
DOI: 10.25165/j.ijabe.20211404.6024

1   Introduction

Severe global water shortage and uneven distribution of water resources have attracted wide attention in the 21st century around the world[1].   Water is a type of indispensable basic resource for national economic and social development[2].   Owing to the limited rainfall and great soil-moisture evaporation, serious water scarcity has widely emerged in the arid and semiarid areas of northwest China, which is one of the major constraints to agricultural production[3].   Therefore, effective utilization of irrigation water under limited precipitation should be considered to increase crop yield while saving water.

Currently, plastic film mulching (PFM) techniques have been widely applied in agricultural practice for grain crops, fruit trees, and vegetable crops[4].   Previous research indicated that plastic film mulching can protect seedlings in arid climates, increase the soil temperature, reduce soil water loss by decreasing evaporation from the soil surface[5,6], control weed growth and prevent nutrient losses from leaching, and increase water use efficiency (WUE) as well as improve crop yield[7].

Film hole irrigation (FHI), as effective water-saving irrigation technology, has been developed on the basis of PFM.   When

irrigating, water flows over the film on the soil surface.   There is a thin layer of water depth above the film hole, and water and fertilizers can be adequately infiltrated into the root zone through the film hole[8].   Meanwhile, FHI can reduce evaporation and deep percolation, which can increase crop yield and economic efficiency[9,10].   FHI has a very promising prospect for widespread application in the irrigation areas of the Yellow River Basin in China[11].   Extensive researches on FHI from the aspects of infiltration characteristics and influence factors have been performed by scholars worldwide[11,12], and some empirical models were established.   Liu et al.[13] showed that PFM led to the volume moisture content increased by 3.5% at depths of 0-20 cm in winter wheat farmland.   Compared with conventional surface irrigation, FHI can save 37%-45% water and increase sunflower yield by 23%-30%[14].   Several fields and laboratory experiments have been carried out to study the effects of influence factors (e.g., soil texture, soil bulk density, film hole diameter, sediment content.) on infiltration characteristics under FHI[15-17].   Dong et al.[18] found that the relationship between the horizontal/vertical wetting front migration distances and infiltration duration was a significant power function.   Jin et al.[19] established a free infiltration model of muddy water film hole irrigation with different initial moisture contents through indoor experiments.   Zhong et al.[20] concluded that in the free infiltration under muddy water irrigation, the cumulative infiltration volume per unit area of film hole, the stable infiltration rate, and the horizontal wetting front migration distance decreased with the increase of the soil bulk density.   Jie et al.[17] established a quantitative model of FHI infiltration process performed indoors with soil boxes, and the simulation model could generally accurately simulate the movement of the wetting front and the changes in the soil moisture volume under FHI.

Most of the irrigation areas are muddy water irrigation areas in the Yellow River Basin of China, and muddy water irrigation primarily occurs in the Yellow River Basin of China[21].   Some

progress has been made in the study of infiltration characteristics of film hole irrigation, but few studies have been conducted on characteristics of water and nitrogen transport under different soil moisture content of muddy water film hole infiltration. Hence, there is a gap in understanding how the muddy water film hole irrigation in combination with different soil moisture content affects soil water and nitrogen transport. The research on soil nitrogen transport and transformation and water fertilizer coupling effect under muddy water film hole irrigation highlights the characteristics and advantages of muddy water FHI in China. Therefore, the objective of this study is to investigate the effects of the initial soil moisture content on soil water and nitrogen transport characteristics under muddy water film hole infiltration and to develop an empirical model for predicting the cumulative infiltration of film hole irrigation. It is anticipated that the findings from this study will provide the theoretical foundation and practical guidelines for applications of film hole irrigation.

2   Materials and methods

2.1   Experimental materials

The experiments were conducted from July to August 2019 at the State Key Laboratory of Eco-hydraulics in Northwest Arid Region, Xi'an, China. The experimental soil samples were taken from Hongqing, Xi'an, in September 2018. The soil samples were collected from the depths of 0-30 cm, air dried and then sieved through a 2-mm sieve. The initial soil moisture content was measured using the oven-drying method. Soil particle composition was determined by using a Mastersizer-2000 laser particle size analyzer. According to the international soil texture classification standards, the soil type used in this experiment was silt loam (30.63% sand, 56.59% silt, and 9.78% clay). The saturated moisture content of the soil sample was about 38%.

According to the soil moisture content in the actual irrigation process, five initial moisture contents (θ_0=6.02%, 7.40%, 8.23%, 10.08%, and 13.20%, mass moisture content, the same below) were employed in the laboratory experiments. The diameter of the film hole was 6 cm, the soil bulk density was 1.30 g/cm^3, and the fertilizer solution (Calcium Ammonium Nitrate, $5Ca(NO_3)_2 \cdot NH_4NO_3 \cdot 10H_2O$) concentration was 600 mg/L. The background values of NO_3^--N and NH_4^+-N, in the soil sample were 6.25 mg/kg and 15 mg/kg, respectively. The sediment concentration of the muddy water was set at 2%.

2.2   Experimental design and method

Figure 1 illustrates the schematic diagram of the experimental set-up. Considering the symmetry characteristics of film hole infiltration, the soil container, composed of 20-mm thick transparent plexiglass, was designed with the internal dimensions of length 30 cm, width 30 cm and height 40 cm. The bottom of the soil container had numerous 2 mm parallel air vents for ventilation, and both sides of the soil container were side holes from which the soil sample could be taken; the diameter of each hole and the distance between the holes were 1 cm and 3 cm, respectively. A Mariotte bottle was fixed with the height adjustable and provided a constant infiltration head for the film hole device through a rubber hose; this bottle had an inner diameter of 9 cm and a height of 100 cm. In order to reduce the deposition of sediment as much as possible, the Mariotte bottle was provided with an automatic agitating system. Blades in the agitating system were driven by an electromotor to revolve, thereby agitating the muddy water. It was calculated that the volume of the blades was only 2‰ of the volume of the Mariotte bottle; the volume of

the blades was thus neglected.
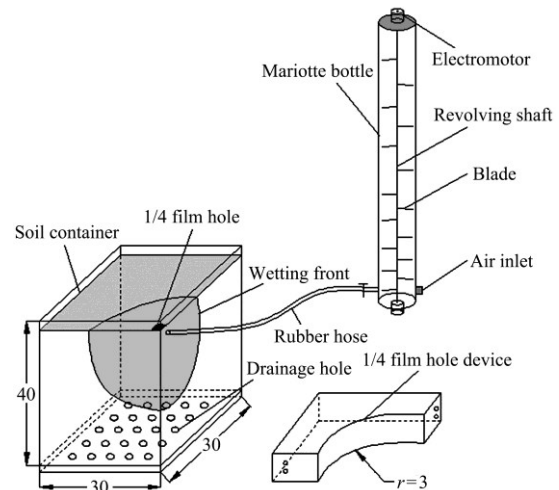
Note: The length, width and height of the soil container are in cm; the radius r of 1/4 film hole device is in cm.

Figure 1   Schematic diagram of experimental set-up

The initial soil moisture content (θ_0) was measured by the oven drying method before the experiment. Before the soil box was filled with soil, transparent adhesive tape was placed on both sides of the soil box to prevent the soil from falling out of the box. The soil was then rammed, based on θ_0 and the predetermined bulk density (1.30 g/cm^3), and by layers (5 cm thick per layer), into the soil container, during which the surface of each soil layer was roughened. Plastic film was used to cover the soil surface and a 1/4 film hole device made of 5 mm thick plexiglass was fixed at one corner of the soil container. The film hole had a radius of 3.0 cm and the film hole device had a water head height of 2.0 cm.

During the experiment, the infiltration duration and the water level in the Mariotte bottle were recorded at progressively prolonged time intervals, and the changes of the wetted body were observed. After the infiltration was over, a soil drill was used to collect soil samples at intervals of 2.5 cm in the horizontal and vertical direction of the film hole center, respectively. Each time the soil of a thickness of 5 cm was collected. Each soil sample was divided into 2 parts, one part was used to measure moisture content, and the other part was used to measure soil NO_3^--N and NH_4^+-N content by a HACH DR/4000 spectrophotometer.

2.3   Data analysis and processing

The statistical analysis software Microsoft Excel 2016 (Microsoft, USA) was used for data processing and analysis. The water content distribution of soil profile was drawn by SURFER 9.0 software program.

Using Excel software, the cumulative infiltration volume per unit film hole area was fitted by the Kostiakov infiltration model[22], which follows:

$$I(t)=Kt^\alpha \qquad (1)$$

where, $I(t)$ is the cumulative infiltration volume per unit film hole area, cm; t is the infiltration duration, min; K is an infiltration coefficient, cm/min$^\alpha$; α is the infiltration index.

3   Results

3.1   Infiltration capacity

3.1.1   Cumulative infiltration per unit film hole area

The cumulative infiltration per unit film hole area ($I(t)$) is shown in Figure 2. $I(t)$ differed greatly under different initial soil moisture content (θ_0), indicating that θ_0 had a significant effect on $I(t)$.
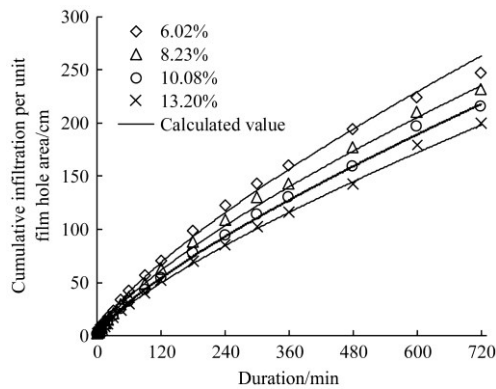
Figure 2   Curves of cumulative infiltration per unit film hole area
under different initial soil moisture contents

The cumulative infiltration volume per unit film hole area $I(t)$ and the infiltration duration (t) was fitted by Equation (1), and the result is shown in Table 1.   The correlation coefficients (R) for all treatments were all larger than the critical correlation coefficient ($R_{0.01}$=0.6614), indicating that the Kostiakov infiltration model could describe the relationship between cumulative infiltration per unit film hole area and infiltration duration.

According to Table 1, K gradually decreased and α gradually increased as the initial moisture content increased.   Specifically, the initial moisture content increased from 6.02% to 13.20%; K decreased from 1.9270 to 1.2324, and α increased from 0.7472 to 0.7721. K reflects the slope degree of the cumulative infiltration curve.   The larger the K is, the greater the slope degree of the

curve is, i.e., the greater infiltration amount.   The α reflects the bending degree of the cumulative infiltration curve, the larger the α is, the smaller the bending degree of the curve is.   It was found that K, α and θ_0 conformed to a linear function relationship, as following:

$$K=-10.1380\theta_0+2.5103, R^2=0.9253 \quad (2)$$
$$\alpha=0.4030\theta_0+0.7218, R^2=0.7522 \quad (3)$$

The coefficients of determination (R^2) of the fitting relationship of Equations (2) and (3) were larger than 0.75.   The Equations (2) and (3) were put into Equation (1), giving a model of the relationship among $I(t)$, t, and θ_0, as following:

$$I(\theta_0,t) = (-10.1380\theta_0 + 2.5103)t^{0.4030\theta_0 +0.7218}, \ 0 \le t \le 720 \quad (4)$$

Equation (4) was used to calculate the cumulative infiltration per unit film hole area ($\theta_0 = 7.40\%$).   Table 2 shows the comparison between calculated and experimental measured values of the cumulative infiltration per unit film hole area, and its relative error values are less than ±7.98%, indicating that Equation (4) could be used to calculate the cumulative infiltration per unit film hole area of muddy water film hole infiltration in different initial moisture contents.

Table 1   Fitted infiltration parameter values

θ_0/%	K/cm·min$^{-\alpha}$	α	R^2
6.02	1.9270	0.7472	0.9946
8.23	1.7184	0.7476	0.9924
10.08	1.3588	0.7716	0.9971
13.20	1.2324	0.7721	0.9949

Table 2   Comparison between calculated and measured cumulative infiltrations (θ_0=7.40%)

Duration/min	30	60	120	180	240	300	360	480	600	720
Measured value/cm	22.52	38.96	66.28	94.76	114.08	139.16	155.88	190.12	223.20	244.00
Calculated value/cm	22.69	38.20	64.31	87.23	108.28	128.05	146.86	182.31	215.60	247.27
Relative error/%	0.74	−1.96	−2.97	−7.95	−5.08	−7.98	−5.79	−4.11	−3.40	1.34

3.1.2   Characteristics of wetting front migration

The variations of the horizontal and vertical wetting fronts are shown in Figure 3a and Figure 3b, respectively.   It can be observed from Figure 3a and Figure 3b that the wetting front continues to advance as the length of time increases, the horizontal and vertical wetting front migration distance increased gradually with the increase of θ_0.   When the water supply was started, the film hole device was immediately filled with water.   Therefore, at the initial stage of infiltration, the horizontal wetting front migration distance rapidly increased to the radius of the film hole, which was significantly larger than the vertical wetting front migration distance.   Because the water infiltrating in the vertical direction was affected by the matrix potential as well as the gravity potential, with the passage of time during the free infiltration of different initial moisture content under the muddy water film hole infiltration, the vertical wetting front migration distance gradually approached the horizontal wetting front migration distance and even exceeded the horizontal migration distance at a time when the infiltration proceeded for about 180 min.

Based on the analysis, it was found that there was a very significant power function relationship between the horizontal and vertical wetting front migration distance and t, as following:

$$F_x=At^B+r \quad (5)$$
$$F_z=Ct^D \quad (6)$$

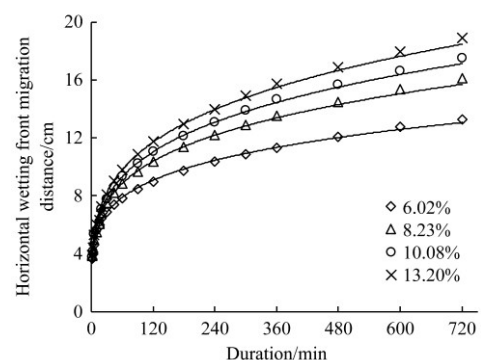where, F_x and F_z are horizontal and vertical migration distance of the wetting front, respectively, cm; A and B are coefficients of migration, cm/min$^\alpha$; C and D are fitting parameters; r is the film

hole radius, r=3 cm.
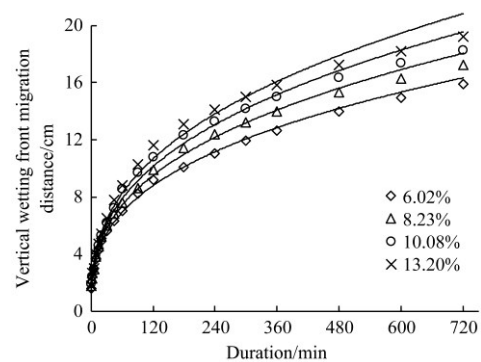
a. Vertical wetting front migration distance

b. Horizontal wetting front migration distance

Figure 3   Curves of the wetting front migration distance

The data from Figure 3a and Figure 3b were fitted with Equations (5) and (6), and listed in Table 3. The coefficients of determination (R^2) were all larger than 0.96, indicating that the power function could adequately describe the relationship between F_x, F_z and t.

Table 3   Fitting parameters of relationship between wetting front migration distance and infiltration time

θ_0/%	$F_x=At^B+3$			$F_z=Ct^D$		
	A	B	R^2	C	D	R^2
6.02	0.8547	0.3986	0.9642	1.6743	0.3461	0.9985
8.23	0.9848	0.4097	0.9865	1.7077	0.3583	0.9968
10.08	0.9773	0.4287	0.9780	1.7500	0.3666	0.9942
13.20	1.0550	0.4296	0.9866	1.7842	0.3734	0.9847

The fitting parameters A, C and B, D were regarded as the coefficient and index of the wetting front migration, respectively. It could be found that A, C and B, D increased significantly with the increase of θ_0 (Figure 4).
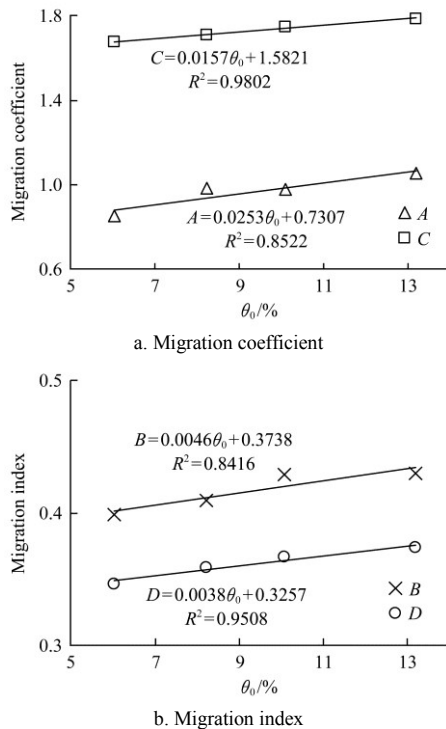

a. Migration coefficient

b. Migration index

Figure 4   Relationship between the wetting front parameters and initial moisture content

According to Figure 4, the coefficients of determination (R^2) in equations about A, B, C and D were larger than 0.8416, indicating that the coefficients A, C and indices B, D of the wetting front migration and θ_0 were significant. By substituting expressions A, B, C and D into Equations (5) and (6), respectively, empirical models about the F_x, F_z and θ_0 could be obtained, as follows:

$$F_x = (0.0253\theta_0 + 0.7037)t^{0.0046\theta_0+0.3738} + r \tag{7}$$

$$F_z = (0.0157\theta_0 + 1.5821)t^{0.0038\theta_0+0.3257} \tag{8}$$

In order to verify the reliability of the above empirical models, the horizontal and vertical wetting front migration distances (θ_0= 7.40%) were calculated by using Equations (7) and (8), respectively. The calculated values were compared with measured values (Figure 5). It could be observed from Figure 5 that the relative errors between the values of the horizontal and vertical migration distances of the wetting front calculated by Equations (7) and (8) and the practically measured values were relatively small, indicating that the empirical models (7) and (8) could predict the vertical and horizontal migration distances.
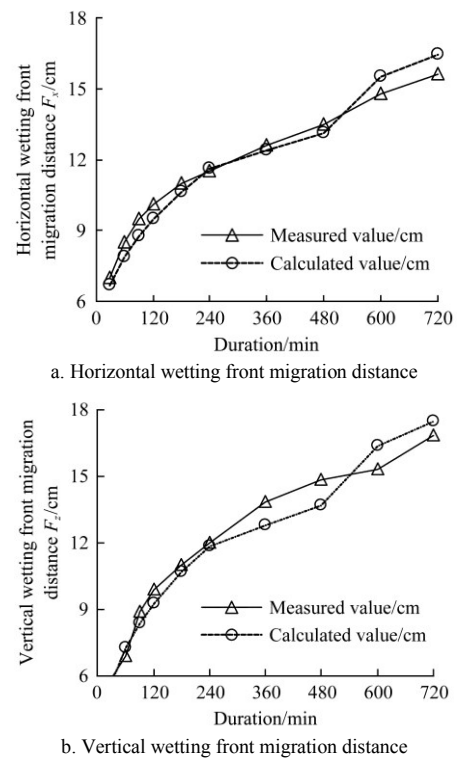

a. Horizontal wetting front migration distance

b. Vertical wetting front migration distance

Figure 5   Comparison of calculated and measured values of horizontal and vertical wetting front migration distances (θ_0=7.40%)

3.2   Moisture content distribution in the wetted body

Due to the axisymmetric nature of the wetted body in the vertical axis direction, soil samples were taken from one side of the soil container to obtain the soil moisture content. The water content distribution was drawn using SURFER 11.0 based on a gridding method called "Kriging" available in the software by taking the film hole center as the starting point (Figure 6). It could be observed from Figure 6 that there was a difference in moisture content distribution of muddy water film hole infiltration in different initial moisture contents, and the moisture content distribution isoline was in the shape of a semi ellipse. The higher the initial soil water content was, the larger the migration rate of the wetting front and the volume of the corresponding wetted body were. At the same time, the higher the initial moisture content was, the higher the moisture content was at the same location in the wetted body.

In order to analyze moisture content distribution in the wetted body, in a more detailed way, the measured data of soil moisture content of redistribution 24 h and 48 h in the vertical direction of the film hole center were analyzed, as shown in Figure 7a and Figure 7b, respectively. Taking the water content in the wetted body at a vertical depth of 15 cm at the film hole center as an example, when θ_0 was 6.02%, 7.40%, 8.23%, 10.08% and 13.20%, the corresponding water content was 10.44%, 13.00%, 14.38%, 15.54%, 20.59%, respectively. If θ_0=6.02% was taken as a benchmark, the increase of water content will be 24.52%, 13.22%, 11.11%, and 48.37%, respectively. This showed that a relatively high initial soil moisture content within a certain range was more conducive to the infiltration of water into the soil. According to Figure 7b, the soil moisture content decreased in the wetted body upper layer, and soil moisture content gradually increased in the

wetted body lower layer.   As the redistribution progresses, the soil moisture content tended to be even distributed in the wetted body. Specifically, the moisture content in the soil within the depth of 0-15 cm decreased significantly and exhibited a tendency of gradually becoming uniformly distributed, which was especially obvious with the soil in the vicinity of the film hole; while the moisture content in the soil within the depth of 15-30 cm showed an increasing trend.   The maximum wetted depths of the wetted body were 16 cm, 22 cm, and 27 cm at the time when the infiltration was over and during the redistribution 24 h and 48 h. At a depth of 10 cm in the vertical direction of the film hole center, the moisture content at the end of the infiltration and during the redistribution 24 and 48 h were 25.47%, 21.46%, and 17.70%, respectively.   If the moisture content in the soil at the end of the infiltration was taken as a benchmark, then the decreases of the moisture content in the soil during the redistribution 24 and 48 h were 15.74% and 30.51%.   The moisture content at a depth of 20 cm at the end of the infiltration and redistribution 24 and 48 h

were 6.02%, 8.61%, and 12.05%, respectively.   If the moisture content in the soil at the end of the infiltration was taken as a benchmark, then the increases of the moisture content in the soil during the redistribution 24 and 48 h were 43.02% and 100.17%. This was mainly because, in the process of redistribution of water in the soil, the water in the wetted body was redistributed under the action of gravity potential and matrix potential, and the soil outside the wetted body was in a state of absorbing water.   Under the action of the water potential gradient, the water continued to move downward and formed a new wetted body.   At the end of infiltration, the soil moisture content was higher within the depth of 0-15 cm, and during the redistribution process, it moved to the surrounding areas with lower water content, and underwent a dehydration process.   The water of soil depth 15-30 cm was supplied thereto by the upper layer of soil, and in the meantime, it also absorbed water through the soil matrix suction.   The moisture content in the soil, therefore, tended to be uniform throughout the wetted body after redistribution 48 h.
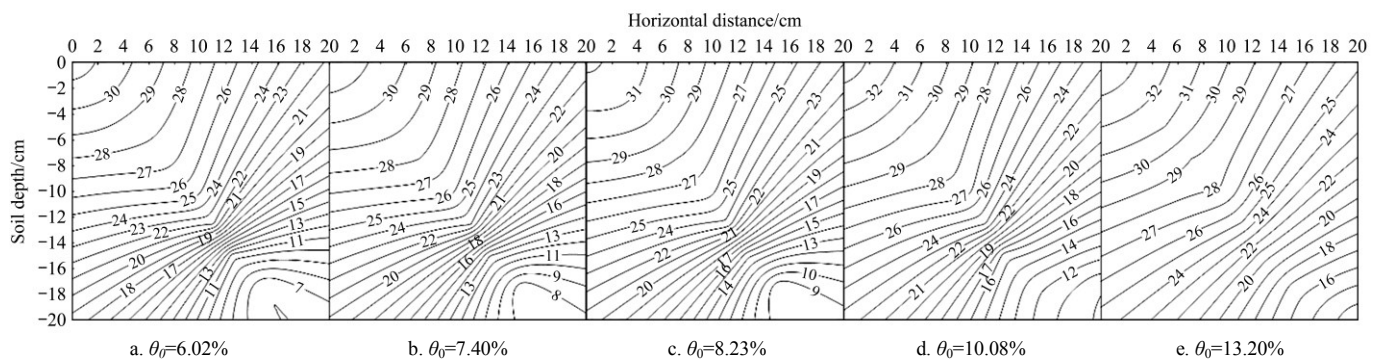

a. θ_0=6.02%   b. θ_0=7.40%   c. θ_0=8.23%   d. θ_0=10.08%   e. θ_0=13.20%

Figure 6   Moisture content distribution in the wetted body at the end of experiments

a. Soil moisture content at the end of the infiltration   b. Soil moisture content after redistribution (θ_0 = 6.02%)
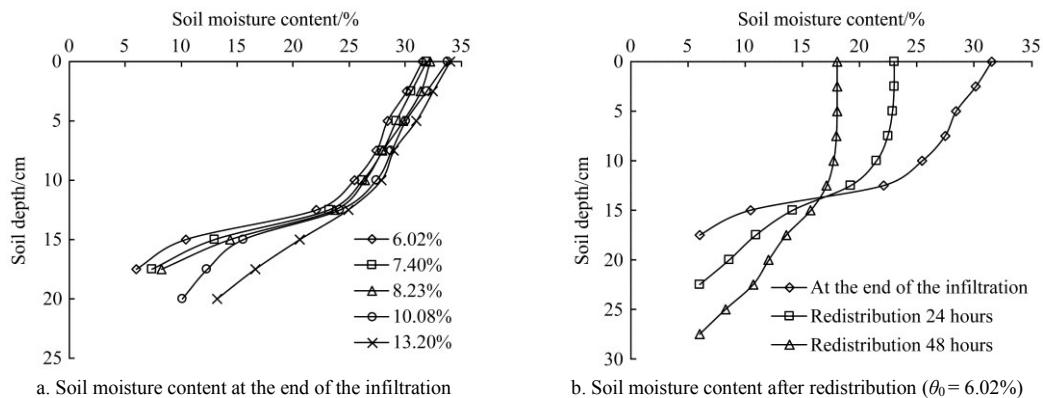
Figure 7   Soil moisture content in the vertical direction of the film hole center

3.3   Transport characteristics of nitrogen in the wetted body

3.3.1   Transport characteristics of NO_3^--N

Figure 8 shows the measured values of NO_3^--N content in the wetted body.   It could be observed from Figure 8a and Figure 8b that the NO_3^--N content increased both in the vertical and horizontal direction with the increase of initial moisture content.   At the center of the film hole, the NO_3^--N content was 44.30, 45.50, 46.01, 46.26, 48.44 mg/kg, respectively; if θ_0=6.02% was taken as a benchmark, then the increases of NO_3^--N content in the wetted body were 2.69%, 1.16%, 0.56%, and 4.93%, respectively.   According to the previous analysis, the higher the initial moisture content was, the greater the cumulative infiltration volume was, the larger the volume of the wetted body was, and the greater the distribution area of NO_3^--N was in the soil of the wetted body.   Within 720 min of infiltration duration, the NO_3^--N was distributed mainly within

15 cm from the film hole under different soil initial moisture content, which further embodied the advantages of the film hole irrigation.   In other words, the fertilizer can be retained in the shallow soil of concentrated distribution in the root area of crops under film hole irrigation, which is not only beneficial to the absorption and utilization of nutrients by crops but also can improve the utilization rate of nitrogen fertilizer.   At the same time, it is not easy to have deep percolation in the process of film hole irrigation, and it can save water and reduce the pollution of NO_3^--N to groundwater.

It can be seen from Figures 8c and 8d that the NO_3^--N contents in the wetted body varied significantly with the proceeding of the redistribution.   In general, with the redistribution of water in the soil, NO_3^--N continued to migrate downward.   Because NO_3^--N and soil colloids have the same charges, which are all negative, NO_3^--N

cannot be easily absorbed by soil colloids, but easily migrate with the diffusion of water. In the process of water infiltration into the soil, the water content in the wetted body decreased gradually with the increase of the distance away from the center of the film hole, and decreased sharply at the wetting front to an extent close to the initial moisture content of the soil. Therefore, the NO_3^--N content in the soil within this range decreases rapidly and almost approaches its background value. In addition, the NO_3^--N content decreased gradually in the upper soil layers, while the lower soil layers formed a new wetted body because of the water redistribution, and the NO_3^--N content thereby increased. Specifically, within redistribution 24 h, within the depth of 0-5 cm, the NO_3^--N contents in the wetted body were almost the same as that at the end of the infiltration. From the water redistribution curves in Figure 7b, it could be seen that the water content in soil decreased significantly within the depth of 0-5 cm and the distribution tended to become gradually even after redistribution

24 h, which indicates that the transport and distribution of NO_3^--N in the wetted body during redistribution 24 h was different from that of water during the infiltration stage. In the infiltration stage, the migration of NO_3^--N was mainly due to the convection effect, but in the process of redistribution, the convection effect was relatively small and therefore the transport of NO_3^--N with the movement of water was not obvious. The NO_3^--N content increased within the depth of 5-30 cm, which was especially obvious in the region of the wetting front. In the soil near the wetting front, the large concentration gradient of NO_3^--N, weak convection, and strong molecular diffusion resulted in the NO_3^--N content increasing significantly. Within redistribution 48 h, the NO_3^--N content within the depth of 0-10 cm decreased significantly compared with the end of infiltration, and the distribution tended to gradually become uniform. In addition, the NO_3^--N content within the depth of 10-30 cm increased, which was consistent with the change of the content of NO_3^--N within redistribution 24 h.

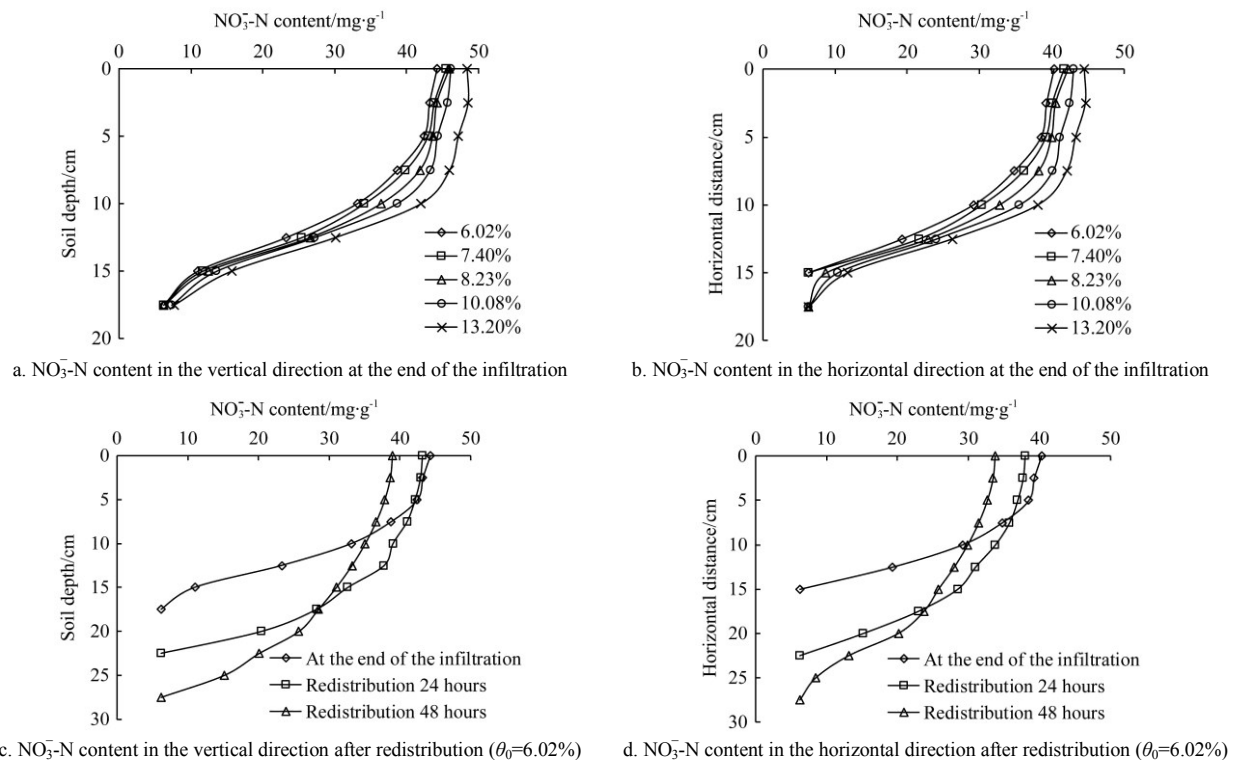a. NO_3^--N content in the vertical direction at the end of the infiltration

b. NO_3^--N content in the horizontal direction at the end of the infiltration

c. NO_3^--N content in the vertical direction after redistribution (θ_0=6.02%)

d. NO_3^--N content in the horizontal direction after redistribution (θ_0=6.02%)

Figure 8   Soil NO_3^--N content in the horizontal and vertical direction of the film hole center

3.3.2 Transport characteristics of NH_4^+-N

Figure 9 shows the measured values of NH_4^+-N content in the wetted body. It could be observed from Figures 9a and 9b that the NH_4^+-N contents in the wetted body were the highest at the film hole center. NH_4^+-N was mainly distributed in the range of 8 cm from the film hole center. In the part of the wetted body that was outside of the 8 cm range, the NH_4^+-N content was significantly reduced. Within the depth of 15-20 cm from the film hole center, although the wetting front arrived, the NH_4^+-N content was not different from the background value of NH_4^+-N in the wetted body. The above phenomenon indicated that the NH_4^+-N distribution in the wetted body was not like the transport of NO_3^--N, i.e., transporting downward with the migration of water in the soil. In other words, the transport of NH_4^+-N did not conform to the general law of solute migration which says "salt comes with water, salt goes with water". The NH_4^+-N in soil solution is positively

charged, while soil colloid is negatively charged. They will attract each other when NH_4^+-N is in contact with soil colloid. In this way, a large amount of NH_4^+-N in soil was adsorbed, and the NH_4^+-N content was thus decreased rapidly, which hindered the migration of NH_4^+-N in soil. In addition, at the same location in the wetted body, the NH_4^+-N contents increased with the increase of the initial moisture content. Under different initial moisture content, the measured NH_4^+-N content in the wetted body at the center of the film hole were 440.40, 453.40, 459.00, 461.70 and 4774.30 mg/kg, respectively. If θ_0=6.02% was taken as a benchmark, then the increases of the NH_4^+-N content were 2.95%, 1.27%, 0.61% and 2.86%, respectively.

It could be seen from Figures 9c and 9d that the NH_4^+-N content changed obviously with the proceeding of the redistribution. Generally speaking, with the proceeding of the redistribution of water in the soil, the wetting front continued to move downward,

and NH_4^+-N in the wetted body also gradually moved downward, and its content showed a decreasing trend.   In the redistribution process, a part of NH_4^+-N in the soil migrated with water, and part of NH_4^+-N underwent a nitration reaction under the action of microorganisms in the soil.   Specifically, within redistribution 24 and 48 hours, within the depth of 0-5 cm, the NH_4^+-N in the wetted body gradually decreased, which was especially obvious in the soil at the center of the film hole; at the end of the infiltration and within redistribution 24 and 48 hours, the NH_4^+-N content in the soil at the center of the film hole were 440.40, 408.58, and 348.90 mg/kg, respectively.   If the NH_4^+-N content at the end of the infiltration

was taken as a benchmark, then the decreases of the NH_4^+-N content in the soil were 7.23% and 20.78%, respectively.   With the proceeding of the redistribution, the distribution of water in the wetted body was more uniform, and the closer it got to the surface of the soil, the better the soil aeration was, which also to some extent promoted the nitrification of NH_4^+-N in the soil.   In addition, the NH_4^+-N content in the soil at the center of the film hole changed a lot because of the loss of NH_4^+-N through volatilization loss. Within the depth of 5-30 cm, the NH_4^+-N content in the wetted body increased gradually.

a. NH_4^+-N content in the vertical direction at the end of the infiltration

b. NH_4^+-N content in the horizontal direction at the end of the infiltration

c. NH_4^+-N content in the vertical direction after redistribution ($\theta_0 = 6.02\%$)

d. NH_4^+-N content in the horizontal direction after redistribution ($\theta_0 = 6.02\%$)
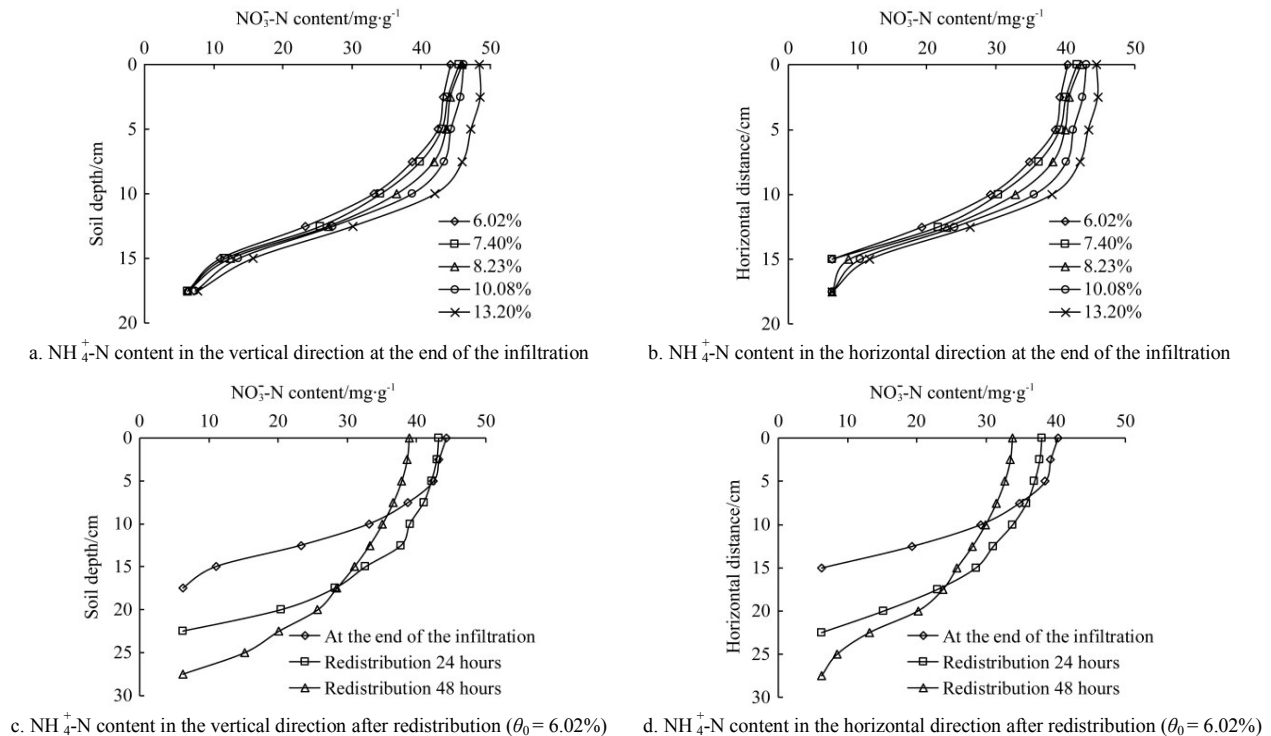
Figure 9   Soil NH_4^+-N content in the horizontal and vertical direction of the film hole center

4   Discussion

The purpose of this study was to investigate the effects of initial moisture content (θ_0) on characteristics of soil water and nitrogen transport under muddy water film hole infiltration. Firstly, based on the laboratory infiltration experiment data, and combined with the boundary characteristics of the test device, a muddy water film fertilizer solution free infiltration model under the experimental setting conditions was developed.   Initial moisture content had a significant effect on soil water and nitrogen transport under muddy water film hole irrigation.   The transport of water and nitrogen in the soil was closely related to soil porosity and nitrogen content[8,16].

In this experiment, the cumulative infiltration per unit film hole area increased with the increase of θ_0.   The functional models of vertical and horizontal distances of wetting front migration were fitted, and the effect of θ_0 on the fitting parameters was revealed. In the process of film hole infiltration, the film hole acted as the only "channel" through which the water entered the soil.   In this way, water infiltrated into the soil under the influence of the film hole chamber water head, and the soil at the center of the film hole was in contact directly with water.   Therefore, the soil near the film hole had the largest water content, which was basically close to saturated water content.   Isolines of moisture content

distribution were relatively sparse, and the change gradient of water content was relatively small.   In addition, in the infiltration of 720 min, NO_3^--N was mainly distributed within a distance of 15 cm away from the film hole center.   This phenomenon further showed the advantage of film hole infiltration, i.e., the fertilizer could be retained in the shallow soil where the root zone of crops was located.   This not only was conducive to the absorption and utilization of nutrients by crops but also could improve the utilization of nitrogen fertilizer[18,23].   In the process of film hole infiltration, water and nutrients hardly leak to deep soil, and film hole infiltration is, therefore, water-saving and can reduce the pollution of NO_3^--N to groundwater[11,24].   However, as this study has only completed the laboratory test, further study is needed for the field application and the parameter optimization of the model.

The Kostiakov model is a relatively classical and traditional theoretical model and is usually used to characterize the process of soil water infiltration[25,26].   The present study applied the Kostiakov model to the simulation of the cumulative infiltration of muddy water film hole infiltration, and the fitting effect of the model was significant, and the coefficient of determination was greater than 0.99.   The conclusions of this study were consistent with the findings of Zhong et al.[27] who have found that the maximum of NO_3^--N content appeared near the film hole center[18]. At the same location, the higher θ_0, the higher average soil

moisture content, which was similar to the results of this study. Moreover, this study is still different from the actual situation and has some limitations. In the actual film hole irrigation, muddy water flows freely along with the film and has the characteristics of flow[15,16]. The emphasis of this paper was on the change of cumulative infiltration and steady infiltration rate with time, that is, the study of the infiltration process. The findings presented in this study might only be suitable and reasonable for the study area investigated, and the model was mainly put forward for specific test conditions, which wasn't universal, but the research method would provide a reference for studies on the infiltration characteristics of film hole irrigation in other regions.

5 Conclusions

In this study, laboratory experiments were conducted with muddy water film hole irrigation, using five initial soil moisture content treatments. The models about 1) the relationship between the cumulative infiltration per unit film hole area ($I(t)$) and infiltration duration (t); 2) the relationship among the horizontal and vertical migration distances of the wetting front (F_x, F_z), θ_0 and t, were established. Kostiakov infiltration model could fit the relationship between $I(t)$ and t. With the increase of θ_0, the infiltration coefficient (K) gradually decreased, but the infiltration index α remains basically unchanged. NO_3^--N was mainly distributed within the range of the wetting radius of 15 cm, while NH_4^+-N was mainly distributed within the range of the wetting radius of 8 cm. This study could provide a theoretical basis and technical support for further study on soil water and nitrogen transport under muddy water film hole irrigation.

Acknowledgements

[References]

[1] Karthe D, Chalov S, Borchardt D. Water resources and their management in central Asia in the early 21 century: status, challenges and future prospects. Environmental Earth Sciences, 2014; 73(2): 487–499.

[2] Swatuk L, Mcmorris M, Leung C, Zu Y. Seeing "invisible water": challenging conceptions of water for agriculture, food and human security. Canadian Journal of Development Studies/Revue Canadienne D'études Du Développement, 2015; 36(1): 24–37.

[3] Deng X P, Shan L, Zhang H, Turner N C. Improving agricultural water use efficiency in arid and semiarid areas of China. Agricultural Water Management, 2016; 80(1–3): 23–40.

[4] Yang J, Mao X M, Wang K, Yang W C. The coupled impact of plastic film mulching and deficit irrigation on soil water/heat transfer and water use efficiency of spring wheat in northwest China. Agricultural Water Management, 2018; 201: 232–245.

[5] Li S E, Kang S Z, Zhang L, Ortega-Farias S, Li F S, Du T S, et al. Measuring and modeling maize evapotranspiration under plastic film-mulching condition. Journal of Hydrology, 2013; 503: 153–168.

[6] Ali S, Xu Y Y, Jia Q M, Ma X C, Ahmad I, Adnan M, et al. Interactive effects of plastic film mulching with supplemental irrigation on winter wheat photosynthesis, chlorophyll fluorescence and yield under simulated precipitation conditions. Agricultural Water Management, 2018; 207: 1–14.

[7] Li R, Hou X Q, Jia Z K, Han Q F, Ren X L, Yang B P. Effects on soil temperature, moisture, and maize yield of cultivation with ridge and furrow mulching in the rainfed area of the Loess Plateau, China. Agricultural Water Management, 2013; 116: 101–109.

[8] Selim T, Bouksila F, Berndtsson R, Persson M. Soil water and salinity distribution under different treatments of drip irrigation. Soil Science Society of America Journal, 2013; 77(4): 1144–1156.

[9] Fan Y W, Gong J G, Wang Y, Shao X X, Zhao T. Application of Philip infiltration model to film hole irrigation. Water Supply, 2019; 19(3): 978–985.

[10] Steinmetz Z, Wollmann C, Schaefer M, Buchmann C, David J, Tröger J, et al. Plastic mulching in agriculture. Trading short–term agronomic benefits for long–term soil degradation? Science of the Total Environment, 2016; 550: 690–705.

[11] Li Y B, Fan Y W, Liu Y, Ma X Y. Influencing factors and simplified model of film hole irrigation. Water, 2017; 9(7): 1–18.

[12] Gupta A D, Babel M S, Ashrafi S. Effect of soil texture on the emission characteristics of porous clay pipe for subsurface irrigation. Irrigation Science, 2009; 27(3): 201–208.

[13] Liu X H, He B L, Yi X, Zhang L G, Han F F. The soil water dynamics and hydraulic processes of crops with plastic film mulching in terraced dryland fields on the Loess Plateau. Environmental Earth Sciences, 2016; 75(9): 1–16.

[14] Saeed M, Mahmood S. Application of film hole irrigation on borders for water saving and sunflower production. Arabian Journal for Science and Engineering, 2013; 38(6): 1347–1358.

[15] Fei L J, Wang J H, Jin S J. Free infiltration characteristics of muddy water film hole irrigation with different film hole diameters. Transactions of the CSAM, 2016; 47(2): 172–178. (in Chinese)

[16] Liu L H, Fei L J, Chen L, Hao K. Effects of sediment concentration of muddy water on water and nitrogen transport characteristics under film hole irrigation with fertilizer infiltration. Transactions of the CSAE, 2020; 36(2): 120–129. (in Chinese)

[17] Jie F L, Fei L J, Zhong Y, Liu L H, Kang S X. Wetting body characteristics and infiltration model of film hole irrigation. Water, 2020; 12(5): 1–14.

[18] Dong Y Y, Mu H W, Fei L J. Experimental study on influence factor under single film hole fertilizer solution infiltration. China Rural Water and Hydropower, 2015; 10: 5–9. (in Chinese)

[19] Jin S J, Fei L J, Fu Y L, Wang J H, Zhong Y, Chen L. Effect of initial soil moisture content on single-line interference infiltration characteristics of muddy water film hole irrigation. Journal of Soil and Water Conservation, 2016; 5: 235–239, 254. (in Chinese)

[20] Zhong Y, Fei L J, Fu Y L, Jin S J, Wang J H. Influence of soil bulk density on single hole point source free infiltration characteristics of muddy water film hole irrigation. Journal of Soil and Water Conservation, 2016; 2: 88–91, 96. (in Chinese)

[21] Yao X, Li J S, Huang X Q, Sun X L. Distribution of Yellow River's silt in field under border irrigation. Transactions of the CSAE, 2016; 32(18): 147–152. (in Chinese)

[22] Kostiakov A N. On the dynamics of the coefficient of water-percolation in soils and on the necessity of studying it from a dynamic point of view for purposes of amelioration. Transactions of 6th Commission of the International Society of Soil Science, Russia, 1932; Part A: 17-21.

[23] Almeida W S D, Panachuki E, Oliveira P T S D, Menezes R D S, Sobrinho T A, Carvalho D F D. Effect of soil tillage and vegetal cover on soil water infiltration. Soil and Tillage Research, 2018; 175: 130–138.

[24] Fan Y W, Shao X X, Gong J G, Wang Y. An empirical model for estimating soil wetting pattern dimensions during film hole irrigation. Archives of Agronomy and Soil Science, 2020; 66(13): 1765–1779.

[25] Fu Q, Hou R J, Li T X, Li Y, Liu D, Li M. A new infiltration model for simulating soil water movement in canal irrigation under laboratory conditions. Agricultural Water Management, 2019; 213: 433–444.

[26] Liu L H, Fei L J, Zhu H Y, Hao K, Jie F L. Study on the influence of fertilizer solution concentration on soil water and nitrogen transport characteristics under film hole irrigation. Journal of Soil Science and Plant Nutrition, 2021; 21: 1653–1665.

[27] Zhong Y, Fei L J, Li Y B. Infiltration characteristics of film hole irrigation under the influence of multiple factor. Irrigation and Drainage, 2020; 69(3): 417–426.